(Supplementary information)

Enhanced Alkaline Bifunctional Electrocatalytic Water Splitting Achieved Through N and S Dual Doped Carbon Shell Reinforced Co_9S_8 Microplates

Mudasir Dar, [a] Kowsar Majid, [a] and Malik Wahid [a*]*

[a]Department of Chemistry
Interdisciplinary Division for Renewable Energy and Advanced Materials (iDREAM),
NIT Srinagar. Srinagar-190006, India.
E-mail: malikwahid15@gmail.com; kowsar@nitsri.in

Number of pages	**12**
Number of figures	**09**
Number of tables	**03**

Calculations:

1. XPS calculations:

XPSPEAK 4.1fitting software was used to analyze individual peak areas to determine the synthesized sample's relative surface elemental composition. Areas (A) enclosed by individual peaks and the relative atomic sensitivity factors (F) of 0.25, 0.66, 0.42, 0.54, and 3.8 for C1s, O1s, N1s S 2p, and Co 2p, respectively, were put in equation S1 to calculate the relative atomic compositions.

Relative atomic % of Z = (Az/Fz) / [(Az/Fz) + (Ay/Fy)] ……Eqn. (S1)

A standard fitting procedure in XPSPEAK 4.1 was adopted to deconvolute individual C1s, O1s, and N1s peaks into their possible functional group peaks by fitting standard binding energy values from the literature.

2. IR-correction, Tafel slope, and overpotential calculations:

The LSV measurements were rectified for electrolyte resistance using equation S2.

$E_{corrected} = E - IR$ ……Eqn. (S2)

Here, I is the measured current (A), R is the uncompensated solution resistance (ohm), and E is the potential applied (V).

The overpotentials (η) are calculated using:

$\eta = E_{corrected} - E_{rev.}$

Where $E_{rev.}$ is the thermodynamic potential (V). On RHE scale, $E_{rev.}$ is 0 V for HER. Therefore, the $E_{corrected}$ is equal to applied η. For OER, the $E_{rev.}$ is 1.23 V vs. RHE, and the η will be

$\eta = E_{corrected} - 1.23\ V$

Tafel plots for HER and OER are obtained from their respective LSV curves, and the Tafel slopes were calculated as per the Tafel equation:

$$\eta = a + b \log j$$

Where a, b, and j represent the Tafel constant, Tafel slope, and current density, respectively.

3. Calculation of Electrochemical active surface area (ECSA):

ECSA was determined using the cyclic voltammetry (CV) technique, involving double-layer capacitance measurement (C_{dl}) of electrocatalysts in the non-Faradiac region. In a typical procedure, carbon fiber modified with an active catalyst acting as a working electrode, Pt mesh, and Ag/AgCl as counter and reference electrodes were used in 1 M KOH solution. CV scans of electrocatalysts were recorded at scan rates of 20, 40, 60, 80, 100, 120, 140, 160, 180 and 200 mV sec^{-1} in a non-Faradiac potential window of 0 - 0.3 V vs. Ag/AgCl electrode. The value of C_{dl} is equal to half of the slope of $\Delta J = (Ja-Jc)$ at 0.15 V vs. scan rate curve. The ECSA was then calculated using the equation:

$$ECSA \approx C_{dl} / C_S$$

Where C_S is the specific capacitance, defined as capacitance per unit area of an atomically smooth planar electrocatalyst surface, the value of C_S is reported as 40 µF in 1 M KOH solution.

Supplementary figures and tables.

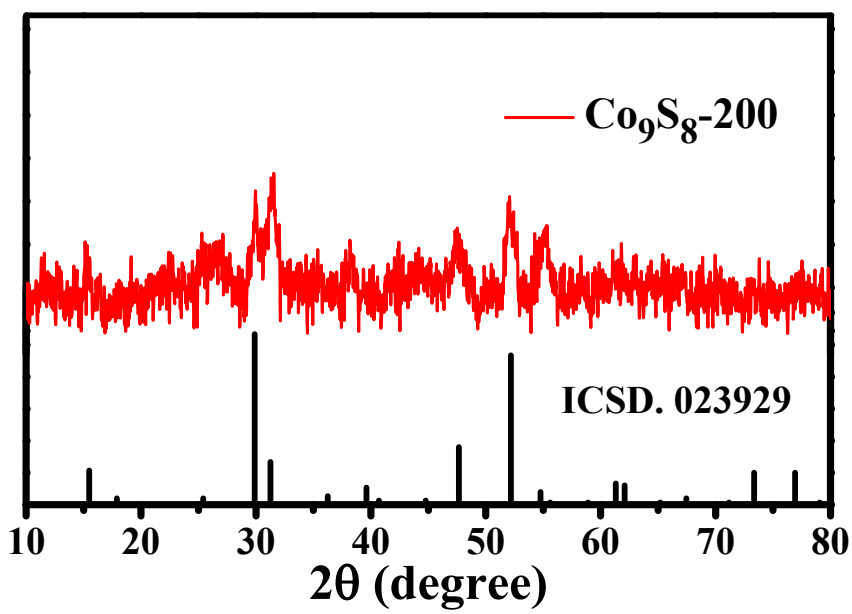

Figure S1. XRD pattern of hydrothermally synthesized Co_9S_8-200 sample

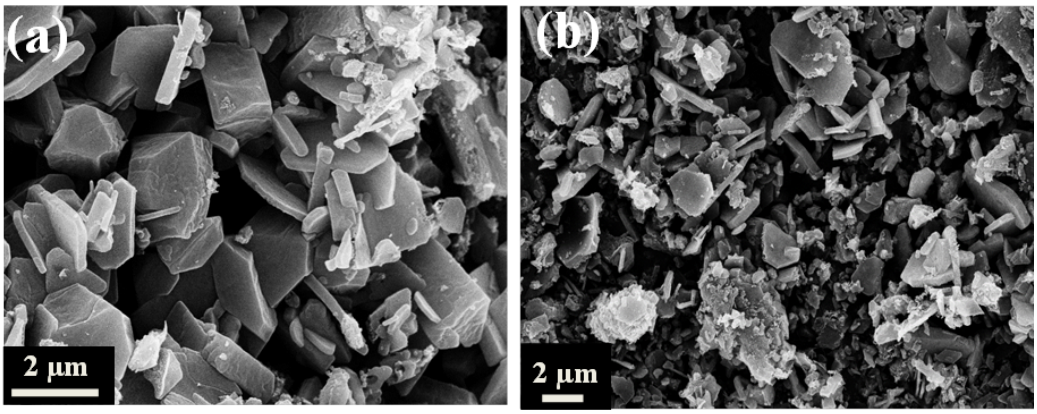

Figure S2. (a) FESEM image of Co_9S_8@NSC-10. (b) FESEM image of Co_9S_8@NSC-6.

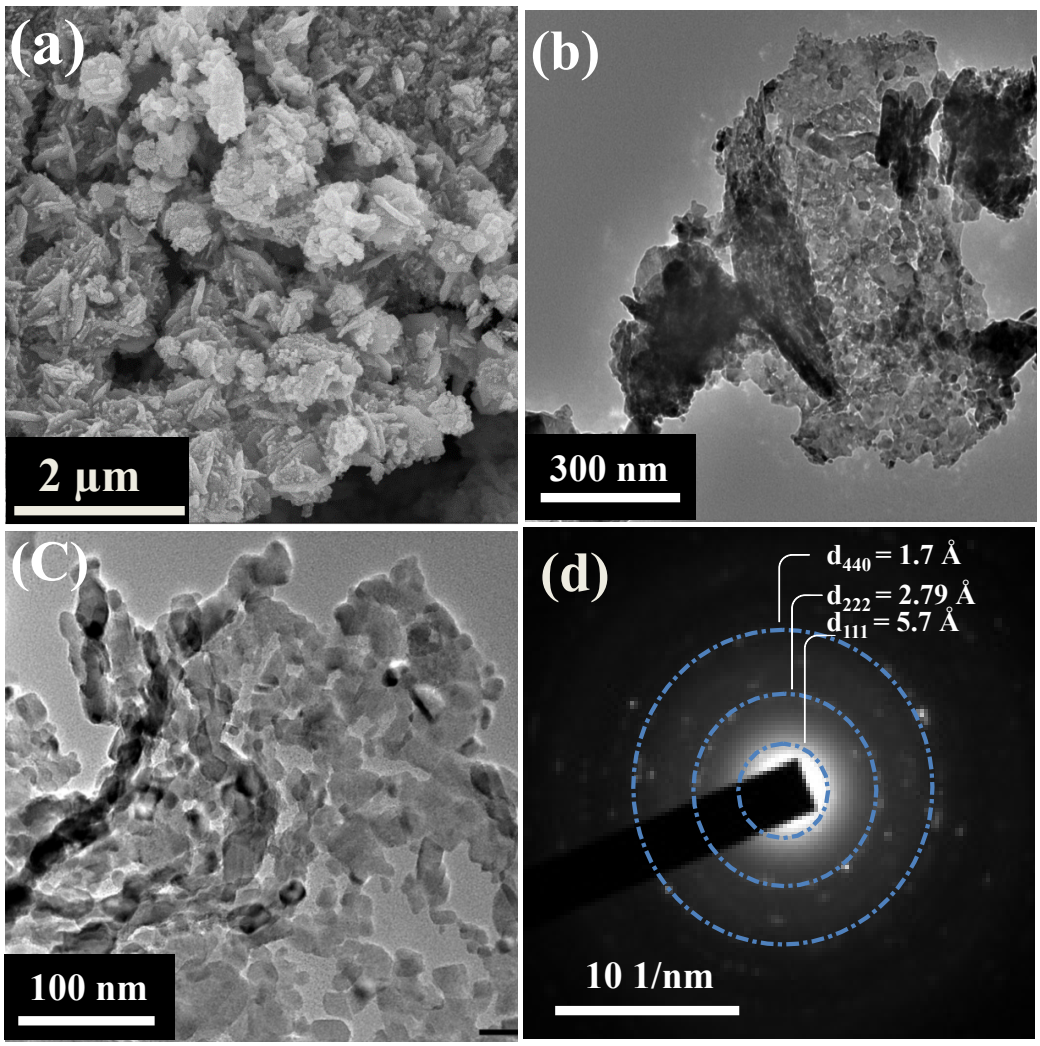

Figure S3. (a) FESEM image of Co_9S_8-800. (b) and (c) HRTEM images of of Co_9S_8-800. (d) SAED pattern of Co_9S_8-800.

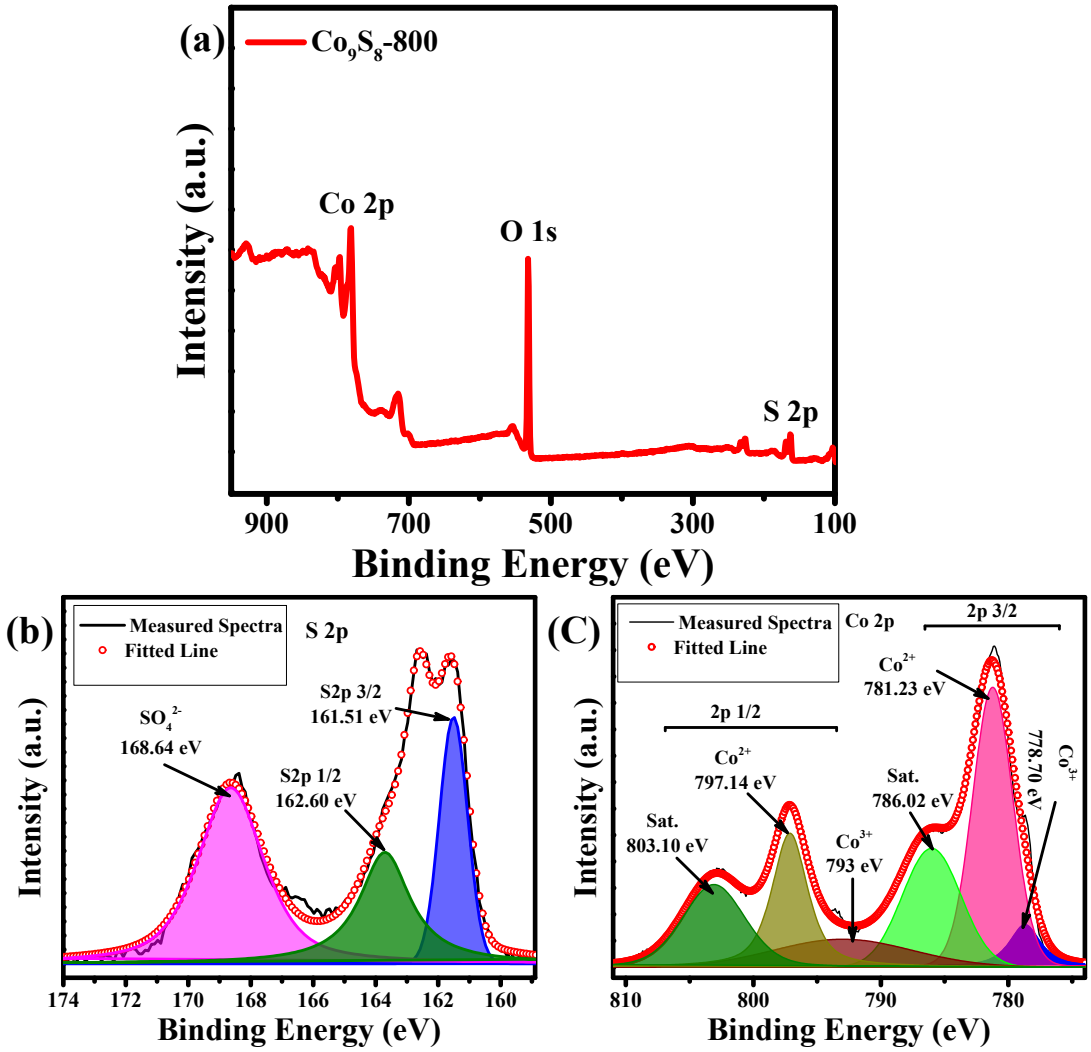

Figure S4. (a) XPS survey spectrum of Co_9S_8; deconvoluted XPS spectra of: (b) S2p, (c) Co 2p of Co_9S_8 material.

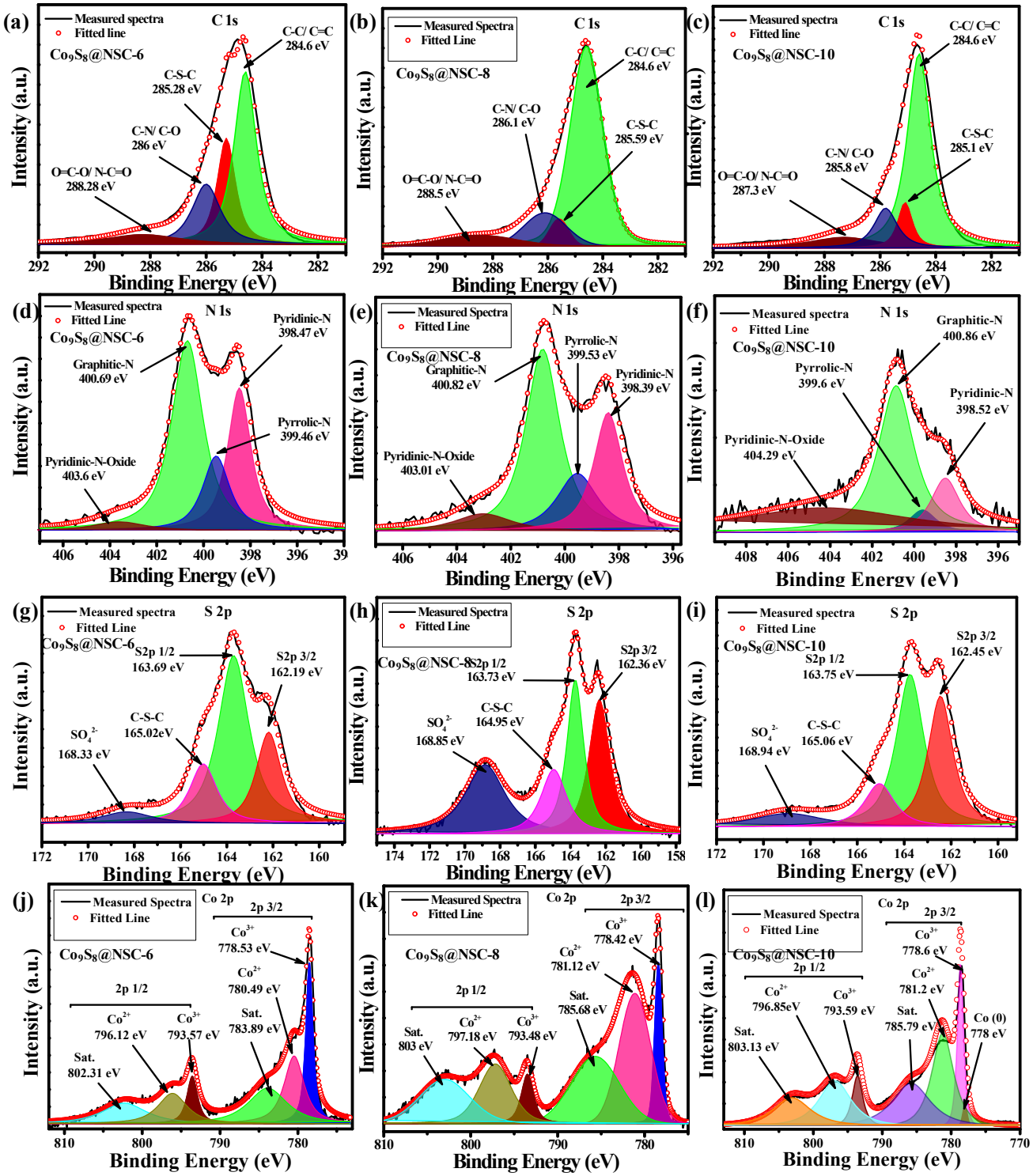

Figure S5. Deconvoluted XPS spectra: (a) C1s of Co_9S_8@NSC-6, (b) C1s of Co_9S_8@NSC-8, (c) C1s of Co_9S_8@NSC-10, (d) N1s of Co_9S_8@NSC-6, (e) N1s of Co_9S_8@NSC-8, (f) N1s of Co_9S_8@NSC-10, (g) S 2p of Co_9S_8@NSC-6, (h) S 2p of Co_9S_8@NSC-8, (i) S 2p of Co_9S_8@NSC-10, (j) Co 2p of Co_9S_8@NSC-6, (k) Co 2p of Co_9S_8@NSC-8, (l) Co 2p of Co_9S_8@NSC-10.

Table S1. XPS functional group analysis of Co9S8@NSC samples.

			Sample		
			Co_9S_8@NSC-6	**Co_9S_8@NSC-8**	**Co_9S_8@NSC-10**
Carbon	C-C/ C=C	Peak Position (eV)	284.6	284.6	284.6
		%	46.9	73.3	66.3
	C-S-C	Peak Position (eV)	285.28	285.59	285.1
		%	23.4	5	9.6
	C-N/ C-O	Peak Position (eV)	286	286.1	285.8
		%	20.6	13.9	13.4
	O=C-O/ N-C=O	Peak Position (eV)	288.28	288.5	287.3
		%	9.1	7.7	10.7
Nitrogen	Pyridinic N	Peak Position (eV)	398.47	398.39	398.52
		%	28.4	26.4	13.4
	pyrrolic N	Peak Position (eV)	399.46	399.53	399.60
		%	17.1	18	5.1
	Graphitic N	Peak Position (eV)	400.69	400.82	399.60
		%	50.7	47.9	45.2
	Graphitic N oxide	Peak Position (eV)	403.6	403.01	404.29
		%	3.8	7.7	36.2

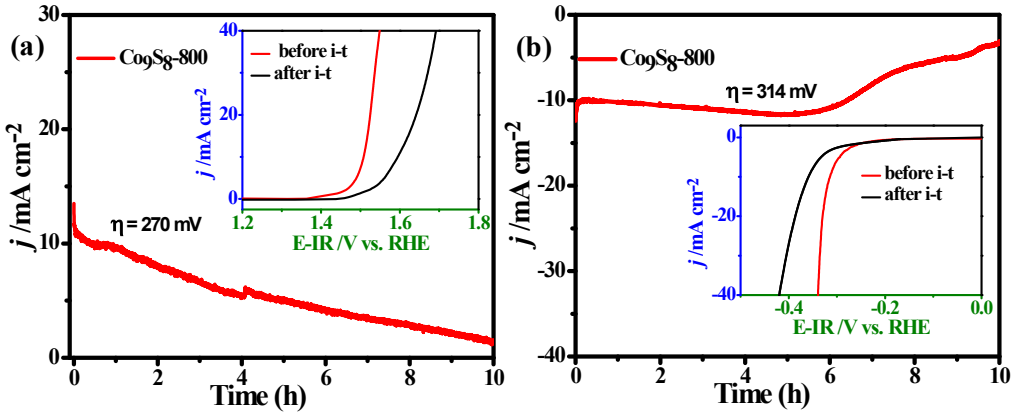

Figure S6. Long-term chronoamperometric (i-t curve) durability test of Co_9S_8-8 in 1 M KOH: (a) for OER at the potential step of 270 mV vs. RHE; inset (a) polarization curves before (red) and after (black) the stability test of Co_9S-8; (b) for HER at the potential step of 314 mV vs. RHE; inset (b) polarization curves before (red) and after (black) the stability test of Co_9S-8

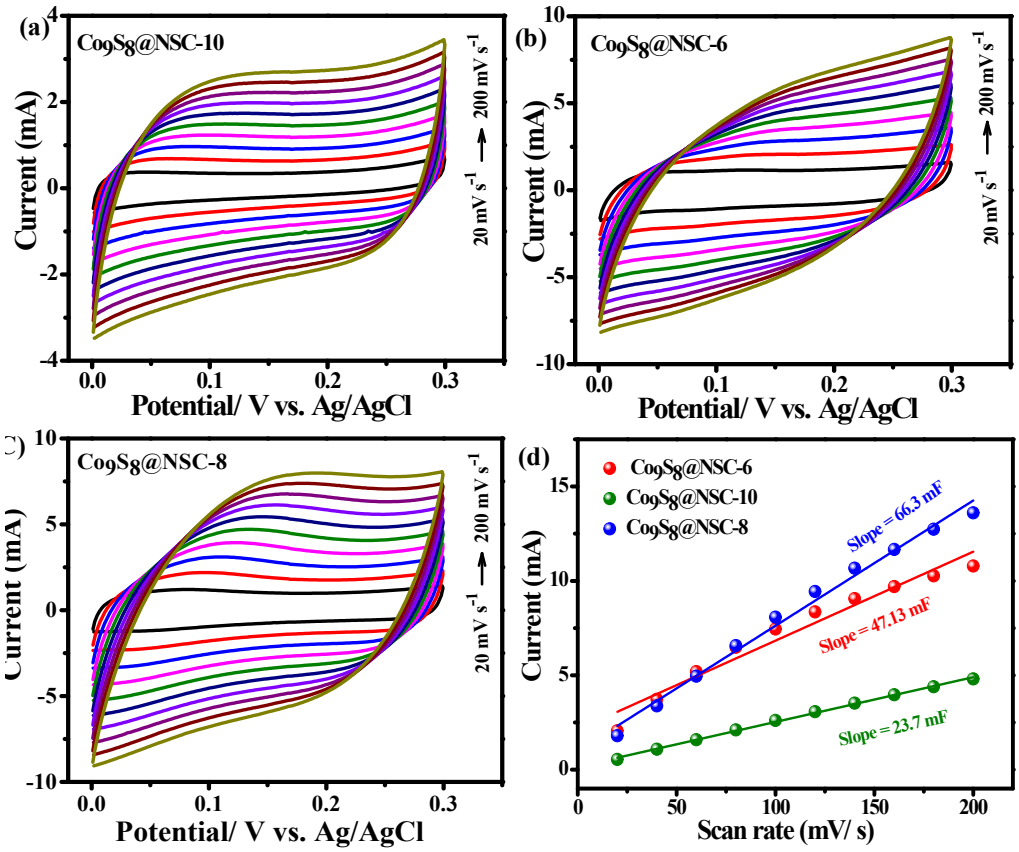

Figure S7. ECSA determination of synthesized electrocatalyst samples in 1 M KOH. Cyclic voltammograms at different scan rates (20-200 mV sec^{-1}) in non-Faradiac region of (a) Co_9S_8@NSC-10; (b) Co_9S@NSC_8-6 and (c) Co_9S_8@NSC-8. (d)The corresponding plot of scan rate vs. current.

Table S2. HER and OER performance of Co_9S_8@NSC and some other noble-metal-free electrocatalysts at 10 mA cm^{-2} in 1.0 M KOH. (j: current density; η: overpotential)

Catalysts	**OER**		**HER**		**Reference**
	η (for J=10 mA cm^{-2}) [mV]	**Tafel Slope [mV dec^{-1}]**	**η (for J=10 mA cm^{-2}) [mV]**	**Tafel Slope [mV dec^{-1}]**	
Co_9S_8@NSC	120	48	267	85	This work
$Ni/Ni(OH)_2$	-	-	300	128	[1]
Porous Co-based film	-	-	375	-	[2]
Co-NRCNT	-	-	370	-	[3]
Co_9S_8@MoS_2/CNFs	430	61	-	-	[4]
FeCoNi-PS	162	-	284	-	[5]
FeCoNi-P	235	-	346	-	[5]
FeCoNi-S	244	-	468	-	[5]
$NiCo_2S_4$ NWs/NF	260	40	210	59	[6]
MoS_2/NiS yolk–shell microspheres	350	108	244	97	[7]
Phosphorene quantum dot/ MoS_2 nanosheets	370	46	600	162	[8]
Co–FeS_2 nanospheres	324	50	267	58	[9]
N-, O-, S-tridoped carbon encapsulated Co_9S_8	340	68	320	105	[10]
Co_9S_8/N,S-rGO	266	75	332	131	[11]
$(Ni_{0.33}Co_{0.67})S_2$ nanowires/ carbon cloth	216	78	334	127	[12]
Ni–Mo–S nanowires	390	75	290	103	[13]
$Co(OH)_2$/Ni–Co–S nanotube arrays	340	64	254	88	[14]
N-carbon coated $NiCo_2S_4$ hollow nanotubes	330	87	295	90	[15]
(210)-Ni_3S_2 nanosheets arrays	260	-	223	-	[16]
NiS microsphere	335	89	158	83	[17]
$Ni(OH)_2/Ni_3S_2$ nanosheets arrays	211	153	270	129	[18]

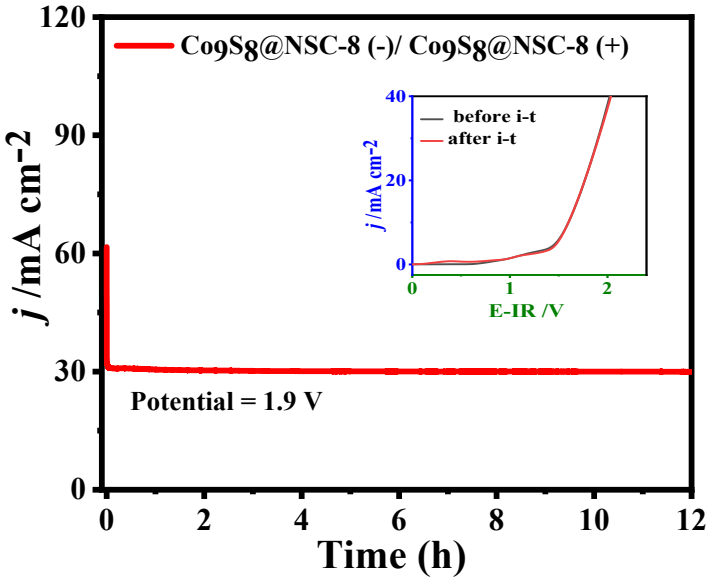

Figure S8. Long-term chronoamperometric (i-t curve) durability test at a potential step of 1.9 V using Co_9S_8@NSC-8 at both electrodes in the two-electrode configuration in 1M KOH, inset depicts Polarization curves before (black) and after (red) stability test of Co_9S_8@NSC-8.

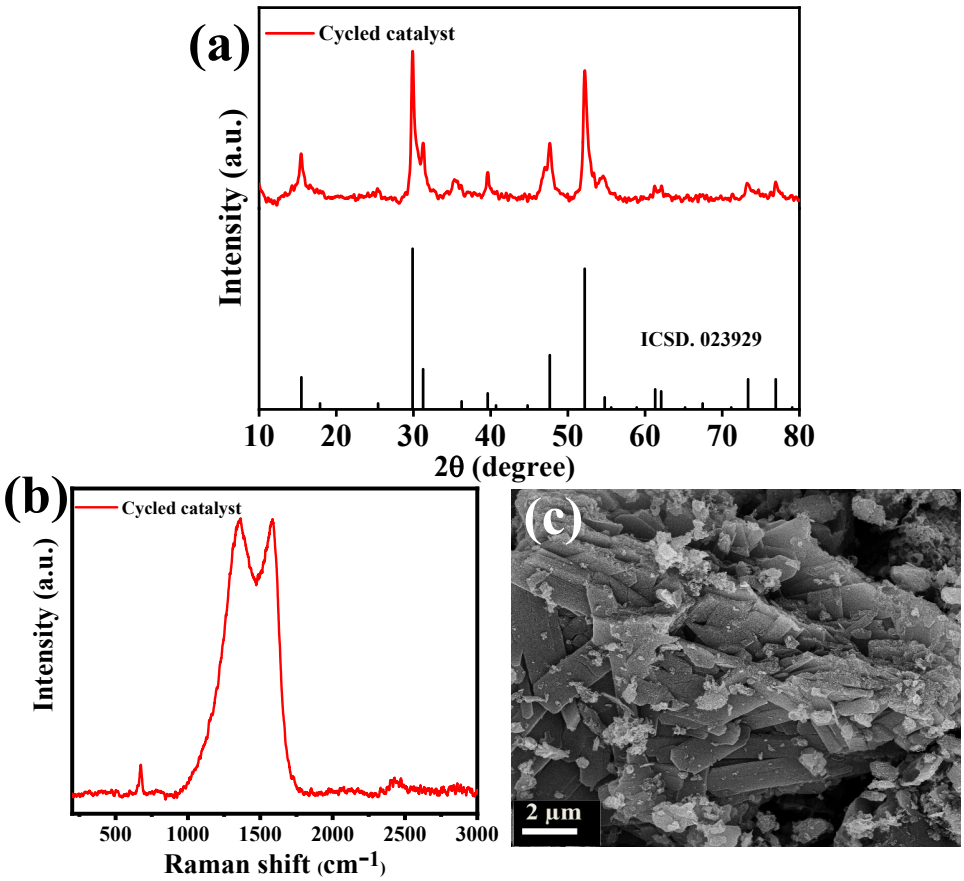

Figure S9. (a) XRD pattern, (b) Raman spectrum, and (c) FESEM image of a sample of Co_9S_8@NSC-8 after being used as an electrocatalyst for water splitting in full-cell configuration in 1M KOH solution at a potential of 1.9 V for 12 h.

Table S3. Comparison of the full cell water-splitting activity of Co_9S_8@NSC catalyst with other reported bifunctional catalysts in basic medium.

Catalysts	Cell Voltage (for J=10 mA cm^{-2}) [V]	Electrolyte	Reference
Co_9S_8@NSC	1.60	1M KOH	This Work
Ni@NC-800/NF	1.60	1M KOH	[19]
NiSe/NF	1.63	1M KOH	[20]
Ni_2P nanowires	1.63	1M KOH	[21]
CoSe film	1.65	1M KOH	[22]
Ni/Mo_2C-PC/NF	1.66	1M KOH	[23]
Ni_5P_4/NF	1.69	1M KOH	[24]
CoP_x/NC	~ 1.71	1M KOH	[25]
Co-P film on Au foil	1.73	1M KOH	[26]
Ni_3S_2/NF	1.76	1M KOH	[27]
Ni(OH)2/NiSe	1.78	1M KOH	[28]
$NiCo_2S_4$ NW/NF	1.63	1M KOH	[29]
CoOSeP@Co	1.74	1M KOH	[30]
RuO_2/ RuO_2	1.45	1M KOH	[31]
RuO_2/Pt-C on CF	1.56	1M KOH	[32]
Ir-C/Pt-C on EG	1.62	1M KOH	[33]
P/Pt	>1.8	1M KOH	[34]
IrO_2/Pt-C	1.6	1M KOH	[35]
Pt-C/Pt-C	1.75	1M KOH	[35]
IrO_2/IrO_2	>1.9	1M KOH	[35]
Pt-C on Ni foam	1.67	1M KOH	[36]
RuO_2/Pt-C both on Ti mesh	1.57	1M KOH	[37]

References:

1 N. Danilovic, R. Subbaraman, D. Strmcnik, K.-C. Chang, A. P. Paulikas, V. R. Stamenkovic and N. M. Markovic, *Angew. Chemie*, 2012, **124**, 12663–12666.

2 Y. Yang, H. Fei, G. Ruan and J. M. Tour, *Adv. Mater.*, 2015, **27**, 3175–3180.

3 X. Zou, X. Huang, A. Goswami, R. Silva, B. R. Sathe, E. Mikmeková and T. Asefa, *Angew. Chemie*, 2014, **126**, 4461–4465.

4 H. Zhu, J. Zhang, R. Yanzhang, M. Du, Q. Wang, G. Gao, J. Wu, G. Wu, M. Zhang, B. Liu, J. Yao and X. Zhang, *Adv. Mater.*, 2015, **27**, 4752–4759.

5 L. Yin, X. Ding, W. Wei, Y. Wang, Z. Zhu, K. Xu, Z. Zhao, H. Zhao, T. Yu and T. Yang, *Inorg. Chem. Front.*, 2020, **7**, 2388–2395.

6 A. Sivanantham, P. Ganesan and S. Shanmugam, *Adv. Funct. Mater.*, 2016, **26**, 4661–4672.

7 Q. Qin, L. Chen, T. Wei and X. Liu, *Small*, 2019, **15**, 1803639.

8 R. Prasannachandran, T. V. Vineesh, M. B. Lithin, R. Nandakishore and M. M. Shaijumon, *Chem. Commun.*, 2020, **56**, 8623–8626.

9 L. Gao, C. Guo, X. Liu, X. Ma, M. Zhao, X. Kuang, H. Yang, X. Zhu, X. Sun and Q. Wei, *New J. Chem.*, 2020, **44**, 1711–1718.

10 S. Huang, Y. Meng, S. He, A. Goswami, Q. Wu, J. Li, S. Tong, T. Asefa and M. Wu, *Adv. Funct. Mater.*, 2017, **27**, 1606585.

11 H. Liu, C. Y. Xu, Y. Du, F. X. Ma, Y. Li, J. Yu and L. Zhen, *Sci. Reports 2019 91*, 2019, **9**, 1–10.

12 Q. Zhang, C. Ye, X. L. Li, Y. H. Deng, B. X. Tao, W. Xiao, L. J. Li, N. B. Li and H. Q. Luo, *ACS Appl. Mater. Interfaces*, 2018, **10**, 27723–27733.

13 Z. Ma, H. Meng, M. Wang, B. Tang, J. Li and X. Wang, *ChemElectroChem*, 2018, **5**, 335–342.

14 F. Wu, X. Guo, G. Hao, Y. Hu and W. Jiang, *J. Solid State Electrochem.*, 2019, **23**, 2627–2637.

15 F. Li, R. Xu, Y. Li, F. Liang, D. Zhang, W. F. Fu and X. J. Lv, *Carbon N. Y.*, 2019, **145**, 521–528.

16 L. L. Feng, G. Yu, Y. Wu, G. D. Li, H. Li, Y. Sun, T. Asefa, W. Chen and X. Zou, *J. Am. Chem. Soc.*, 2015, **137**, 14023–14026.

17 W. Zhu, X. Yue, W. Zhang, S. Yu, Y. Zhang, J. Wang and J. Wang, *Chem. Commun.*, 2016, **52**, 1486–1489.

18 X. Du, Z. Yang, Y. Li, Y. Gong and M. Zhao, *J. Mater. Chem. A*, 2018, **6**, 6938–6946.

19 X. Wang, W. Li, D. Xiong and L. Liu, *J. Mater. Chem. A*, 2016, **4**, 5639–5646.

20 C. Tang, N. Cheng, Z. Pu, W. Xing and X. Sun, *Angew. Chemie Int. Ed.*, 2015, **54**, 9351–9355.

21 L. A. Stern, L. Feng, F. Song and X. Hu, *Energy Environ. Sci.*, 2015, **8**, 2347–2351.

22 T. Liu, Q. Liu, A. M. Asiri, Y. Luo and X. Sun, *Chem. Commun.*, 2015, **51**, 16683–16686.

23 Z.-Y. Yu, Y. Duan, M.-R. Gao, C.-C. Lang, Y.-R. Zheng and S.-H. Yu, *Chem. Sci.*, 2017, 968–973.

24 M. Ledendecker, S. Krickcalderõn, C. Papp, H. P. Steinrück, M. Antonietti and M. Shalom, *Angew. Chemie Int. Ed.*, 2015, **54**, 12361–12365.

25 B. You, N. Jiang, M. Sheng, S. Gul, J. Yano and Y. Sun, *Chem. Mater.*, 2015, **27**, 7636–7642.

26 J. A. Vigil and T. N. Lambert, *RSC Adv.*, 2015, **5**, 105814–105819.

27 L. L. Feng, G. Yu, Y. Wu, G. D. Li, H. Li, Y. Sun, T. Asefa, W. Chen and X. Zou, *J. Am. Chem. Soc.*, 2015, **137**, 14023–14026.

28 H. Liang, L. Li, F. Meng, L. Dang, J. Zhuo, A. Forticaux, Z. Wang and S. Jin, *Chem. Mater.*, 2015, **27**, 5702–5711.

29 A. Sivanantham, P. Ganesan and S. Shanmugam, *Adv. Funct. Mater.*, 2016, **26**, 4661–4672.

30 Y. F. Jiang, C. Z. Yuan, X. Zhou, Y. N. Liu, Z. W. Zhao, S. J. Zhao and A. W. Xu, *Electrochim. Acta*, 2018, **292**, 247–255.

31 Y. Dang, T. Wu, H. Tan, J. Wang, C. Cui, P. Kerns, W. Zhao, L. Posada, L. Wen and S. L. Suib, *Energy Environ. Sci.*, 2021, **14**, 5433–5443.

32 W. Li, X. Gao, D. Xiong, F. Xia, J. Liu, W. G. Song, J. Xu, S. M. Thalluri, M. F. Cerqueira, X. Fu and L. Liu, *Chem. Sci.*, 2017, **8**, 2952–2958.

33 Y. Hou, M. R. Lohe, J. Zhang, S. Liu, X. Zhuang and X. Feng, *Energy Environ. Sci.*, 2016, **9**, 478–483.

34 M. Ledendecker, S. Krickcalderõn, C. Papp, H. P. Steinrück, M. Antonietti and M. Shalom, *Angew. Chemie Int. Ed.*, 2015, **54**, 12361–12365.

35 N. Jiang, B. You, M. Sheng and Y. Sun, *Angew. Chemie Int. Ed.*, 2015, **54**, 6251–6254.

36 C. Tang, N. Cheng, Z. Pu, W. Xing and X. Sun, *Angew. Chemie Int. Ed.*, 2015, **54**, 9351–9355.

37 J. Tian, N. Cheng, Q. Liu, X. Sun, Y. He and A. M. Asiri, *J. Mater. Chem. A*, 2015, **3**, 20056–20059.